Treatment of fluoroacetate by a *Pseudomonas fluorescens* biofilm grown in membrane aerated biofilm reactor

Running title: Treatment of fluoroacetate in a MABR

Barry Heffernan[1], Cormac D. Murphy[2], Eoin Syron[1] and Eoin Casey[1]*.

[1]UCD School of Chemical and Bioprocess Engineering and [2]UCD School of Biomedical and Biomolecular Science, Centre for Synthesis and Chemical Biology,
University College Dublin, Belfield, Dublin 4, Ireland.

*Corresponding Author: Eoin Casey.
Address: UCD School of Chemical and Bioprocess Engineering, Engineering and Materials Science Centre, University College Dublin, Belfield, Dublin 4, Ireland.
Email: eoin.casey@ucd.ie
Telephone: +353 1 7161877
Fax: +353 1 7161177

Abstract

Fluorinated organic compounds have widespread applications, and their accumulation in the environment is a concern. Biofilm reactors are an effective technology for the treatment of contaminated wastewater, yet almost no research has been conducted on the effectiveness of biofilms for the biodegradation of fluorinated aliphatic compounds. In this paper we describe experiments undertaken to investigate the degradation of fluoroacetate using a membrane aerated biofilm reactor (MABR) by *Pseudomonas fluorescens* DSM8341. The concentration of fluoroacetate in the medium influenced biofilm structure, with less dense biofilm observed at lower fluoroacetate loading rates. As biofilm thickness increased, oxygen utilisation decreased, probably as a consequence of increased resistance to oxygen transfer. Furthermore, most of the biofilm was anaerobic, since oxygen penetration depth was less than 1000 μm. Biofilm performance, in terms of fluoroacetate removal efficiency, was improved by decreasing the fluoroacetate loading rate however, increasing the intra-membrane oxygen pressure had little effect on biofilm performance. A mathematical model, showed that while fluoroacetate does not penetrate the entire biofilm, the defluorination intermediate metabolite glycolate does, and consequently the biofilm was not carbon limited at the biofilm-membrane interface where oxygen concentrations were highest. The model also showed the accumulation of the free fluoride ion within the biofilm. Overflow metabolism of glycolate was identified to be most likely a result of a combination of oxygen limitation and free fluoride ion inhibition. The study demonstrated the potential of MABR for treating wastewater streams contaminated with organofluorine compounds.

Introduction

Fluorine is amongst the most abundant elements in the earth's crust [1], however most of this terrestrial fluorine is bound in an insoluble form and thus biologically unavailable [2]. As a result of this unavailability and the physicochemical properties of the fluoride ion, the occurrence of natural fluorinated organics is rare, with about a dozen isolated to date. However, over the past 50 years the presence of synthetic fluorinated organics in industrial wastewater streams has increased substantially due to the increased use of fluorine as a substituent in many pharmaceuticals and agrochemicals [3]. Despite this increase in the use of fluorine few studies have investigated the fate of fluorinated compounds in biological wastewater systems.

Fluoroacetate is a highly toxic substance and is used as a vertebrate pest control agent. It is also a metabolite of a number of other compounds, such as fluoroacetamide, which is used to control rodents; the anticancer drugs 5-fluorouracil and fluoroethyl nitrosourea, and the industrial chemical fluoroethanol [4-6]. This transformation of other fluorinated compounds to fluoroacetate offers an explanation for the presence of low concentrations of fluoroacetate in fog and rain samples from northeast Bavaria [7]. A wide variety of microorganisms isolated from soil samples have shown the ability to defluorinate fluoroacetate [8, 9]. The microbial degradation of fluoroacetate is now well understood at the mechanistic level specifically the fluoroacetate dehalogenase enzyme isolated from *Moraxella* sp B [10]. Although the microbial degradation of fluoroacetate has been extensively studied, few researchers have investigated the degradation of fluoroacetate or any other aliphatic fluorinated compounds in biofilm reactors.

The membrane aerated biofilm reactor (MABR) is a promising technology for the treatment of wastewater streams. This technology has been under investigation at laboratory scale for several decades [11] and very recently has a dedicated commercial system been

developed [12]. In the MABR the biofilm naturally immobilize to an oxygen permeable membrane. Oxygen is supplied through this membrane into the biofilm where oxidation of pollutants, supplied at the biofilm-liquid interface, takes place. In the context of wastewater treatment the MABR has three main advantages over conventionally aerated reactors: first it is possible to achieve high volumetric chemical oxygen demand (COD) removal, second, high oxygen utilization efficiencies are attainable, and third, as a result of the unique microbial stratification profile in MABRs it is possible to achieve simultaneous nitrification, denitrification and COD removal in a single biofilm reactor[13]. MABRs can also reduce stripping-loss of volatile organic wastewater constituents such as acetonitrile [14]. The MABR configuration also has a number of advantages from a practical research point of view; including the ability to measure biofilm thickness and oxygen utilization rates non-invasively. To date most MABR studies have concentrated on total nitrogen removal [15], simultaneous carbonaceous/nitrogen removal [16] and the treatment of volatile wastewater constituents [17]. The degradation of fluorinated compounds in a MABR has not previously been studied.

Pseudomonas fluorescens is commonly found in environmental soil and water samples, in the food processing industry, in drinking water distribution systems and on plant surfaces where it exists in commensal relationships with plants [18, 19]. The specific strain used here, *P. fluorescens* (DSM 8314), was previously isolated from a soil sample in Western Australia and was shown to have the ability to degrade fluoroacetate as the sole carbon source [20].

Due to the increased presence of fluorinated compounds in industrial wastewater streams and the limited research on the ability of biological wastewater treatments systems to treat fluorinated compounds, it is of general and practical interest to study the ability of a MABR-grown *P. fluorescens* biofilm to degrade fluoroacetate. The objective of this work was to examine the long-term performance of a *P. fluorescens* biofilm grown in a MABR

100 with fluoroacetate as the sole carbon source. A mathematical model was used to determine
101 the metabolite profiles in the biofilm for various intra-membrane oxygen pressures and bulk
102 liquid fluoroacetate concentrations.
103

104 Materials and Methods

105 **Medium and culture conditions**.

106 *Pseudomonas fluorescens* (DSM 8341) was obtained from the German Collection of
107 Microorganisms and Cell Cultures (DSMZ, Germany). Brunners minimal medium (DSMZ,
108 medium 457) supplemented with sodium fluoroacetate as the sole carbon source was the
109 growth medium for all experiments except where otherwise stated. This medium contains no
110 nitrite or nitrate, which some pseudomonads can use as a terminal electron acceptor in the
111 absence of oxygen, thus under these conditions, the bacterium can only grow aerobically.

112 **Bioreactor configuration**

113 A schematic of the MABR system used is shown in Figure 1. A silicone tube (Alteil^{TM}, UK)
114 of outer diameter 3.0 mm and wall thickness 1 mm with an active length of 300 mm was
115 fitted coaxially in a glass tube (QVF, Germany) of inner diameter 15 mm. The medium was
116 continuously recirculated between the membrane module and a 50 cm^3 syringe via a gear
117 pump (Cole Parmer, USA). The syringe served as a compact mixing vessel and was fitted
118 with four ports at the top for feed addition, spent medium removal, and two ports for
119 recirculating medium between the syringe and the membrane module. A bottom port was
120 used for daily sampling of the liquid for the measurement of fluoroacetate, free fluoride ion,
121 glycolate, dissolved oxygen, pH and CFUs. Mixing in the syringe was achieved by the
122 flowrate of the liquid (0.77 L/min) returning from the membrane module.
123 The temperature of the system was controlled at 30 ± 1 ºC by means of a heating coil
124 connected to a water bath. Pure oxygen (Air Products, Ireland) with purity > 99.5% was

supplied at an elevated pressure (0.25-0.75 bar gauge) to the membrane lumen. A continuous flow of approximately 6 ml/min was maintained to remove any water vapor or gasses, which could back-diffuse into the membrane. The septa shown in Figure 1 were used for microsensor measurements. The feed flow rate was measured by recording the mass of liquid effluent over a specified period of time using a balance ± 0.5 g (Mettler Toledo, USA). The reactor was checked daily for contamination by plating an effluent sample on Tryptone Soya Agar.

Bioreactor operation

Two separate runs were undertaken in the MABR corresponding to 10 (reactor I) and 20 (reactor II) mM fluoroacetate in the medium feed. Prior to operation the reactor system was autoclaved at 121ºC for 15 min. All liquid medium was autoclaved prior to use to prevent contamination and to ensure pure culture conditions. Prior to reactor inoculation cells were grown for 24 h at 30 ºC in batch culture to ensure the cells were in the exponential phase of growth. An inoculum (10 ml) of this 24 h culture was adjusted to an optical density of approximately 0.1 at 660 nm in phosphate-buffered saline (PBS) and used to inoculate the MABR. The system was operated in static mode for approximately 48 h after which time the flow of medium was initiated at a flow rate of 30 ml/h and maintained throughout the biofilm accumulation phase of the experiment. In both cases the intra-membrane oxygen pressure was 0.25 bar gauge during the biofilm accumulation phase. The effect of intra-membrane oxygen pressure on performance was assessed under continuous flow conditions at a constant fluoroacetate loading rate of 0.64 mM/h. The reactor was operated at steady state for 72 h at each intra-membrane pressure and sampled three times during this time frame. The effect of different fluoroacetate loading rates on performance was assessed under continuous flow conditions at a constant intra-membrane pressure was 0.50 bar. The reactor was operated at steady state for 72 h at each intra-membrane pressure and sampled three times during this

time frame. Prior to any perturbation in intra-membrane oxygen pressure or loading rate, the reactor was operated at a loading rate of 0.64 mM/h and an intra-membrane pressure of 0.50 bar for 24 h. Finally, reactor II was temporarily converted to batch mode to examine the effect of different staring concentrations of fluoroacetate. The reactor was operated at steady state conditions for at least 48 h prior to a batch experiment, following which the feed rate was increased to 200 ml/min for 5 min (approximately 5 washouts). The feed was then stopped for the duration of the batch experiment. Biofilm thickness was 3700 μm and the intra-membrane pressure was 0.50 bar for the batch experiments.

Biofilm thickness

The biofilm thickness method, which is based on imaging the cylindrical biofilm through the glass walled vessel, has been previously described by Syron et al [21]. Approximately 80 mm of the biofilm was captured in each image and the overall diameter of the biofilm was then measured at 12 points along this length. As the biofilm is annular in cross-section it was useful to linearise thickness in order to make biofilm accumulation rate more meaningful, using the equation $\zeta = (r_0 + \delta)\ln\left(\frac{r_0 + \delta}{r_0}\right)$ where δ is the recorded thickness and r_o is the radius of the silicone tube, the biofilm accumulation rate was then calculated from this value.

Oxygen transfer/utilization rate This method has previously been described by [22] and is based on the principle that the change in pressure of oxygen in a temporarily sealed membrane lumen is proportional to the flux of oxygen through the membrane walls. This is a rapid and non-invasive method but necessitates the use of pure oxygen instead of air.

Oxygen penetration

Oxygen concentration profiles in the biofilm were measured using a needle type oxygen microsensor (PreSens, Germany). The needle type oxygen sensor had a tip size of 50 μm and a response time of 1 s. The oxygen sensor was connected to a Microx TX3 oxygen meter

(PreSens, Germany) and the dissolved oxygen concentration was recorded on a computer. The microsensor was calibrated using a two-point calibration, in an air-saturated environment and in an oxygen free environment obtained by immersing the tip in a sodium sulfite saturated solution. The oxygen sensor was then mounted on an adapted microscope and oxygen profiles were obtained by moving the oxygen sensor through the septum and into the biofilm every ten seconds in 10 μm increments by use of a manually controlled stepping motor. Single measurements were taken in reactor II on days 103, 107 and 111 corresponding to intra-membrane oxygen pressures of 0.25, 0.50 and 0.75 bar oxygen.

Fluoroacetate, free fluoride ion and glycolate analysis

Free fluoride ion was measured using an ion selective fluoride combination electrode (Thermo Orion model 290). Fluoroacetate concentration was determined by fluorine-19 nuclear magnetic resonance (^{19}F NMR). Samples were prepared by mixing 0.6 ml of culture fluid with 0.2 ml D_2O (added to provide a lock signal) and analysis was performed using a Varian 400 MHz spectrometer. The known free fluoride concentration in each effluent sample was used as an internal standard. The ratio of free fluoride ion signal (δ -120 ppm) to fluoroacetate signal (δ -215 ppm) was used to calculate fluoroacetate concentration. Glycolate was measured by a colorimetric method involving boiling the sample in dihydroxynaphthalene and sulphuric acid as described by Lewis and Weinhouse [23].

Mathematical Model for MABR

The objective of the model was to determine the metabolite profiles in the biofilm for various intra-membrane oxygen pressures and bulk liquid fluoroacetate concentrations. The degradation of fluoroacetate in the MABR resulted in elevated levels of the intermediate metabolite glycolate and free fluoride ion. Carbon is conserved in the fluoroacetate dehalogenase reaction, which results in the production of glycolate and free fluoride ion, thus, ultimately glycolate serves as the carbon source for the biofilm. Accordingly, a steady-state

reaction-diffusion model, previously described by [21], was modified to consider the degradation of fluoroacetate, the production of glycolate and free fluoride ion and the utilization of oxygen and glycolate in the MABR. Biofilm thickness (measured) was an input into the model and growth and decay were not explicitly modeled. For a more detailed description see supplemental information.

Results

Biofilm formation and structure

A qualitative assessment of the outer surfaces of the biofilms formed in the 10 mM (reactor I) and 20 mM (reactor II) reactors were homogeneous in structure (Supplemental Fig 2). However, as biofilm thickness increased the reactor I biofilm became more heterogeneous with the formation of streamer structures, which were not present in reactor II. This heterogeneity was also reflected in the standard deviation from the mean mature biofilm thickness, which was ± 596 μm in reactor I (mean thickness of 4287 μm), compared with ± 273 μm in reactor II (mean thickness 3878 μm).

Biofilm growth

No sloughing events were observed during the experiments, and erosion, as indicated by optical density measurements, was minimal, the optical density remained ≤ 0.005 at 660 nm after initial biofilm formation. Thus it was possible to calculate biofilm accumulation rates from thickness measurements. Figure 2 shows that there were four distinct phases of biofilm accumulation for both reactors with the fastest phase (phase A, 0.053 h^{-1}) occurring when the biofilm thickness was less than 300 μm. Thereafter, a concomitant decrease in the rate of biofilm accumulation occurred as biofilm thickness increased (phase B, 0.012 h^{-1}, phase C, 0.004 h^{-1}, and phase D, 0.002 h^{-1}).

Effect of biofilm thickness on oxygen transfer/utilization rates

223 The dissolved oxygen concentration in the effluent was measured daily and after initial
224 biofilm formation remained below detection throughout the biofilm accumulation phase of
225 growth. Thus, as oxygen did not penetrate from the biofilm into the bulk liquid, all the
226 oxygen transferred across the membrane can be considered to have been utilized by the
227 biofilm, and consequently the oxygen transfer rate is equivalent the oxygen utilization rate.
228 The effect increasing biofilm thickness had on the oxygen utilization rate is shown in Figure
229 3; during phase A of biofilm growth oxygen utilization rates increased as the biofilm
230 thickness increased, this increase was probably a result of increased oxygen demand due to
231 the increased biomass in the MABR. The oxygen utilization rate then decreased during phase
232 B of biofilm accumulation for both reactors. This decrease in oxygen utilization rate can be
233 attributed to the increased resistance to oxygen transfer caused by the increased biofilm
234 thickness. Oxygen utilization rates reached a steady state of approximately 9 g/m^2/day for
235 both reactors during phase C of biofilm accumulation.

236 The biofilm thickness at which reactor I switched from the B phase of growth to the C
237 phase of growth was 2300 μm, approximately 1000 μm thicker than when reactor II
238 switched. At similar biofilm thicknesses the oxygen transfer rate was higher for reactor I
239 compared to reactor II. This suggests that the resistance to mass transfer was greater for
240 reactor II than reactor I. This is consistent with the visual observation suggesting biofilm in
241 reactor I is less dense that in reactor II.

242 **Oxygen penetration depth profiles**

243 While the absence of dissolved oxygen in the effluent after initial biofilm formation
244 demonstrates that oxygen did not completely penetrate the biofilm, it does not give any
245 indication as to the actual oxygen penetration depth. Figure 4A shows oxygen penetration
246 depths as measured using the microsensor at three different intra-membrane oxygen pressures
247 in reactor II. Increased intra-membrane pressure resulted in an increased dissolved oxygen

concentration at the membrane substratum. However, varying the intra-membrane oxygen pressure did not have any noticeable effect on oxygen penetration depth. For all three pressures, oxygen penetration was less that 1000 μm into the biofilm from the membrane substratum in the fully developed biofilm. This resulted in an anaerobic zone over 2500 μm in thickness which acts as a substantial diffusive barrier to the transport of fluoroacetate and glycolate to the zone of respiratory activity.

The model was used to predict oxygen profiles at intra-membrane oxygen pressures of 0.25, 0.5 and 0.75 bar (Fig 4B). There was good agreement between the predicted and measured oxygen profiles at these three intra-membrane oxygen pressures. The model predicts that the oxygen penetration depth is largely independent of intra-membrane oxygen pressure at a biofilm thickness of 3700 μm, which is in agreement with measured oxygen penetration depths.

Effect of intra-membrane oxygen pressure on biofilm performance

The effect of varying intra-membrane pressure on the performance of the biofilm was also examined (Table 1). There was no statistically significant difference in the fluoroacetate utilization rate at the three intra-membrane pressures ($p>0.05$), with approximately 6.5 mM of fluoroacetate remaining in the effluent at all three pressures. Consequently the biofilm performance in terms percentage fluoroacetate removed was also unaffected by increases in intra-membrane oxygen pressure. However, increased intra-membrane oxygen pressure resulted in a statistically significant increase in the oxygen utilization rates ($p<0.05$). While there was no statistically significant difference in the glycolate utilization rate at the three intra-membrane pressures there was an overall decreasing trend with decreasing pressure, suggesting that a significant difference might be observed over a broader range of pressures.

Effect of biofilm thickness on fluoroacetate and glycolate utilization rates

The performance of the reactors during biofilm formation and growth was assessed in terms of fluoroacetate and glycolate utilization rates. Utilization rates were defined as the concentration of substrate degraded per unit time and calculated in terms of mM/h carbon for comparison purposes. Both reactors were operated with a feed flow rate of 30 ml/h, thus the fluoroacetate loading rate of 0.30 mM/h in reactor I was half the loading rate of that in reactor II (0.60 mM/h). The fluoroacetate and glycolate utilization rates remained constant in both reactors during initial biofilm formation and growth (first 600 h of biofilm growth), as indicated by standard deviation around the mean measurements. The fluoroacetate utilization rate was 0.32 ± 0.04 mM/h for reactor I and 0.41 ± 0.1 mM/h for reactor II. There was very little difference between the glycolate utilization rates recorded in both reactors, which were 0.24 ± 0.02 and 0.21 ± 0.07 mM/h for reactors I and II, respectively. An increased glycolate utilization rate could have been expected in reactor II considering more glycolate was produced in this reactor. This was not the case and suggests a rate limitation for glycolate utilization, which did not affect fluoroacetate utilization.

There was almost complete fluoroacetate utilization in reactor I after 400 h of biofilm growth, with approximately 1 mM of fluoroacetate remaining in the effluent. In reactor II approximately 10 mM of fluoroacetate was degraded by a 400 h old biofilm, however, there was still 8 mM of fluoroacetate remaining in the effluent. Overflow metabolism of glycolate resulted in an increased glycolate concentration in the effluent in both reactors. The higher fluoroacetate loading rate in reactor II resulted in higher concentrations of glycolate and free fluoride in the effluent of reactor II (Fig 5).

Biofilm performance under alternative fluoroacetate loading rates

The effect of fluoroacetate loading rate on reactor performance was assessed in reactor II (Table 2). Three different fluoroacetate loading rates were assessed (0.64, 0.40 and 0.32 mM/h). There was no statistical difference in fluoroacetate and glycolate utilization rates

297 between the 0.64 and 0.40 mM/h loading rates ($p>0.05$) however, biofilm performance in
298 terms of fluoroacetate removal efficiency was improved from 61.0 % at the 0.64 mM/h
299 loading rate to 89.5 % at the 0.40 mM/h loading rate. A further reduction of the fluoroacetate
300 loading rate to 0.32 mM/h resulted in a statistically significant reduction the fluoroacetate,
301 oxygen and glycolate utilization rates in comparison to the 0.64 mM/h loading rate ($p<0.05$) .
302 Fluoroacetate removal efficiency at the 0.32 mM/h loading rate (91.5 %) was only marginally
303 improved in comparision to the 0.40 mM/h loading rate. However, both fluoroacetate and
304 glycolate were almost completely degraded at the 0.32 mM/h loading rate, with only 1.7 and
305 2.6 mM of fluoroacetate and glycolate, respectively, remaining in the effluent. Thus it was
306 possible to improve reactor performance, in terms of fluoroacetate removal efficiency and
307 substrate remaining in the effluent, by decreasing the fluoroacetate loading rate.

308 There was a statistically significant decrease in oxygen utilization rates at the 0.32 and
309 0.40 mM/h fluoroacetate loading rates in comparison with the 0.64 mM/h fluoroacetate
310 loading rate ($p<0.05$). There are two possible explanations for this result: either the decreased
311 fluoroacetate loading rate results in decreased availability of glycolate and thus a decreased
312 oxygen demand, or there is consolidation within the biofilm. Consolidation results in
313 compacting of the biofilm due to a combination of decreased activity within the biofilm and
314 the pressure exerted by the fluid velocity on the biofilm[24]. If consolidation does occur it is
315 likely to increase the resistance to oxygen transfer.

316 **Steady state predicted metabolite profiles**

317 Ideally the profiles of fluoroacetate, glycolate and free fluoride ion within the biofilm at the
318 different fluoroacetate loading rates would have been measured. However, at present there
319 are no microsensors available to measure these parameters. Thus, a mathematical model was
320 developed to predict their profiles in the biofilm.

The predicted profiles of fluoroacetate, glycolate, oxygen and free fluoride ion concentrations at three experimental fluoroacetate loading rates of 0.32, 0.40 and 0.64 mM/h are shown in Figure 6. Fluoroacetate, glycolate, and free fluoride ion boundary conditions at the bulk liquid biofilm interface were set to experimental conditions while the oxygen concentration at the membrane biofilm interface were also set to experimental values. Overall, increasing bulk liquid fluoroacetate concentration resulted in an increased fluoroacetate penetration depth, increased glycolate and free fluoride ion concentrations at the biofilm membrane interface, but had little effect on oxygen penetration depth.

The fluoroacetate penetration depth into the biofilm from the bulk liquid decreased by 1300 μm when the fluoroacetate loading rate was decreased from 0.64 to 0.32 mM/h. Oxygen penetration depth from the membrane substratum into the biofilm was largely independent of the fluoroacetate loading rate with a marginal decrease (200μm) in penetration depth from the membrane when the fluoroacetate loading rate was decreased from 0.64 to 0.32 mM/h. The overflow metabolism of glycolate within the biofilm resulted in elevated concentrations of glycolate within the biofilm with the peak glycolate concentration located in a region approximately 1000 to 1500 μm from the biofilm-membrane interface. Glycolate can then diffuse both towards the oxygen rich region adjacent to the membrane where it can be utilized, but also towards the bulk liquid and the region of biofilm where oxygen is absent; glycolate cannot be utilized in this region.

Free fluoride ion inhibition of glycolate utilization was included in the model. The model predicts elevated free fluoride ion concentration of up to 35 mM within the biofilm, with the highest concentrations located at the biofilm membrane interface. The glycolate concentrations at the biofilm-membrane interface were approximately 3 and 7 mM for the loading rates of 0.40 and 0.64 mM/h, respectively. Thus, a higher glycolate utilization rate could have been expected at the 0.64 mM/h fluoroacetate loading rate, this was not observed

(Table 2). However, the increased fluoroacetate loading rate also results in an increased free fluoride ion concentration at the biofilm membrane interface, and this offers an explanation as to why no increase in glycolate utilization rate was observed when there was an increased glycolate concentration at the biofilm membrane interface.

Dimensionless activity is defined as the ratio between the predicted growth in a region of the biofilm and the maximum possible growth if all substrates are available in excess. The highest activity at each of the fluoroacetate loading rates examined was located towards the biofilm-membrane interface where both oxygen and glycolate are present for all fluoroacetate loading rates examined. The activity at the membrane interface decreases as the fluoroacetate loading rate decreases, as a result of the decreased glycolate concentration at this location. It is possible the decreased oxygen transfer rates observed for the 0.40 and 0.32 mM/h fluoroacetate loading rates are a result of decreased activity, which might increase the density of the biofilm in this region, and thus increase resistance to mass transfer through the process of consolidation.

Effect of step changes in the fluoroacetate loading rate on biofilm performance

The ability of the *P. fluorescens* biofilm to cope with step changes in the fluoroacetate loading rate was examined under batch conditions in both reactors. Fluoroacetate concentrations of 10, 20 and 50 mM were examined in reactor II only (Fig 7). The degradation of fluoroacetate results in the production of glycolate, and the release of fluoride and H^+ ions. While this H^+ ion has the potential to decrease pH, the KH_2PO_4 concentration in the medium was found to be adequate to buffer the system (pH 6.5) throughout the experiment when the loading rate was 0.64 mM/h or less. The buffering capacity of the medium was also adequate for the batch experiments when the initial fluoroacetate concentrations were 10 and 20 mM. However, when the initial fluoroacetate concentration was 50 mM (Fig 7 C) the pH dropped to 4.9, which prevented the utilization of fluoroacetate

and glycolate and resulted in severely decreased oxygen transfer rates. Accordingly, the concentration of KH_2PO_4 was increased from 1.52 to 15.2 g/l to provide greater buffering capacity. As a result of this increase in KH_2PO_4 concentration, the pH remained between 6.5 and 6.9 throughout the time course of the buffered 50 mM fluoroacetate batch experiment (Fig 7 D). Fluoroacetate was completely utilized after 8, 18 and 27 h for the 10, 20 and buffered 50 mM experiments respectively. Overflow metabolism of glycolate was evident in all experiments and a significant amount of glycolate remained in the bulk liquid after fluoroacetate had been completely utilized in all the experiments. While the initial oxygen utilization rate was high in all experiments, the rate decreased as fluoroacetate was utilized in the 10 and 20 mM experiments. This decrease did not occur in the buffered 50 mM experiment.

Discussion

Fluorinated compounds are extensively used in many applications (refrigeration, plastics, electronics, pharmaceuticals, insecticides and herbicides) and can be considered significant environmental contaminants. To date there has been limited research on the degradation of fluorinated compounds in biological reactor systems and here the ability of a *P. fluorescens* biofilm to degrade the model xenobiotic fluoroacetate was studied in a MABR.

In membrane-attached biofilm systems, biofilm thickness is of major importance in determining process performance [25], the experimental system used in this study permitted biofilm accumulation to be measured throughout by means of biofilm thickness measurements. Biofilm accumulation is the net change in biomass associated with growth, decay and detachment. In the experiments reported here, the detachment rate in the MABR, due to erosion, was observed to be at a minimal and constant level throughout biofilm formation (optical density approximately 0.005 at 660 nm), while major sloughing events

396 were absent. The absence of sloughing events, which are a common occurrence in biofilm
397 systems, maybe explained by a combination of shear stress and the low biofilm growth rate
398 observed here. A mathematical model[26] has demonstrated, detachment to be, in part,
399 dependent on growth rate and liquid shear stress and it was suggested that higher growth rates
400 trigger instability in biofilm accumulation, which results in abrupt biofilm loss while higher
401 shear was demonstrated to produce higher strength biofilms. The fastest biofilm accumulation
402 rate recorded in the MABR was 0.053 h^{-1}, this accumulation rate is considerably lower than
403 the maximum planktonic growth rate 0.16 h^{-1} [27] and combined with the fluid velocity in the
404 membrane module of 1.2 cm/s provides a possible explanation as to why no major sloughing
405 events were observed through the time course of the experiments.
406 Four distinct phases of biofilm growth were observed (Fig 2) the fastest rates of
407 biofilm accumulation were recorded when the biofilm was less than 300 μm, thereafter the
408 rate of biofilm accumulation decreased. The highest oxygen utilization rates during biofilm
409 growth were also recorded when the biofilm thickness was less than 300 μm (Fig 3). When
410 the biofilm thickness was less than 300 μm, diffusional limitations are likely to be minimal.
411 Thereafter they increase with increasing biofilm thickness. Thus, diffusional limitations offer
412 an explanation for this decreased growth and the decreased oxygen utilization rates observed
413 with increased biofilm thickness. The final biofilm thickness in reactor I was greater than in
414 reactor II, even though the fluoroacetate loading rate was higher in the latter. Structural
415 difference in the biofilm composition may explain this. A number of studies have shown how
416 nutrient concentrations control the morphology of biofilms [28, 29], at higher nutrient
417 concentrations biofilms are thicker and denser than under nutrient-poor conditions. Biofilm
418 images show streamer structures in reactor I that were not present in reactor II. Streamer
419 structures have also been shown at lower substrate loading rate [29], which disappeared or were
420 difficult to distinguish at higher loading rates. Here streamers resulted in an increased average

biofilm thickness but also increased the heterogeneity, as indicated by standard deviation around the mean thickness measurements. Oxygen utilization rates during biofilm formation support the possibility that there were structural difference between the two reactors. More glycolate was produced in reactor II than in reactor I, thus, higher oxygen utilization rate could have been expected in reactor II. However, this was not observed and higher oxygen utilization rates were recorded in reactor I. Suggesting that the biofilm formed in reactor I was less dense than the biofilm formed in reactor II. It is also possible that the higher free fluoride concentrations recorded in reactor II could have contributed to the structural differences observed between the two reactors. Since the concentration of free fluoride is in excess of the Ca^{2+} and Mg^{2+} concentrations (0.3 and 0.8 mM, respectively in the medium) it could potentially sequester these cations, which are known to influence biofilm formation directly through their effect on electro-static interactions and indirectly via physiology dependent attachment processes by acting as important cellular cations and enzyme cofactors [30].

The data show the accumulation (overflow metabolism) of glycolate in both reactors with concentrations of up to 6 mM of glycolate measured in reactor II (Fig 3). Thus, the rate of glycolate catabolism is slower than the rate of fluoroacetate dehalogenation. Oxygen limitation has been suggested as an explanation for this overflow metabolism of glycolate in a tubular biofilm reactor [27]. In that study staining with the respiratory indicator CTC (5-cyano-2,3-ditoyl tetrazolium chloride) suggested the possibility of oxygen limitation within the biofilm. Donnelly and Murphy [31] have shown that the *P. fluorescens* fluoroacetate dehalogenase enzyme degrades fluoroacetate in the absence of oxygen, thus fluoroacetate degradation is not rate limited by oxygen. However, the utilization of glycolate via aerobic respiration requires oxygen as an electron acceptor. In the present study oxygen penetration profile measurements showed that there were large anaerobic zones of approximately 2500

446 μm within the biofilm, supporting the possibility that oxygen is the rate limiting step (Fig
447 4A). The fluoroacetate, glycolate and oxygen utilization rates at varying intra-membrane
448 pressures (Table 1) also support the possibility that oxygen is the rate limiting step in
449 glycolate utilization. The fluoroacetate utilization rate did not change significantly with
450 increasing intra-membrane oxygen pressure, however, glycolate and oxygen utilization rates
451 increased suggesting glycolate utilization is more dependent on oxygen than fluoroacetate.

452 The model was developed in order to estimate the general trends in the metabolite
453 spatial profiles within the biofilm under the experimental conditions undertaken and to help
454 test hypotheses regarding metabolite utilisation patterns and possible inhibition. Based on
455 experimental observation in this study and a previous study [27] oxygen limitation was
456 modelled as the rate limiting step of glycolate utilization. However, oxygen limitation alone
457 did not predict the accumulation of glycolate within the biofilm but did predict elevated
458 concentrations of free fluoride ion at the biofilm membrane interface. A number of studies
459 investigating the effects of fluoride on dental biofilms have also shown accumulation of
460 fluoride within the biofilms [32, 33]. Furthermore [34] have suggested that high concentrations of
461 free fluoride ion might sequester Mg^{2+} and Ca^{2+} limiting their availability for other important
462 cellular processes. Consequently, non competitive inhibition of glycolate utilization by free
463 fluoride ion was included in the model. An increased glycolate utilization rate could have
464 been expected at the fluoroacetate loading rate of 0.64 mM/h as the glycolate concentration at
465 the membrane interface is approximately 5 mM higher at the biofilm membrane interface
466 compared to when the fluoroacetate loading rate was 0.40 mM/h (Fig 6). However, this was
467 not the case and the model can be used to explain this observation. The model shows the
468 accumulation of free fluoride ion at the biofilm membrane interface where glycolate and
469 oxygen concentrations are highest at all three fluoroacetate loading rates. The highest
470 concentrations of free fluoride ion (approximately 35 mM) were predicted at the fluoroacetate

471 loading rate of 0.64 mM/h and offer an explanation as to why an increased glycolate
472 utilization rate was not observed at this loading rate.

473 The glycolate utilization rate at the fluoroacetate loading rates of 0.64 and 0.40 mM/h
474 are approximately the same. Consequently, similar oxygen utilization rates could have been
475 expected at these loading rates as the utilization of glycolate via aerobic respiration is the
476 main driving force for the transfer of oxygen across the membrane. This was not the case and
477 the oxygen utilization rate at the fluoroacetate loading rate of 0.64 mM/h was significantly
478 higher than at the 0.40 mM/h loading rate. Consolidation could explain this result; it has been
479 suggested that certain conditions, such as diminished biomass activity, result in the structural
480 realignment of the biofilm to form higher density, lower porosity biofilms [24]. The model
481 predicts decreased glycolate and consequently decreased activity at the biofilm membrane
482 interface for the 0.40 mM/h loading rate suggesting the possibility of consolidation, which
483 could result in an increased mass transfer resistance to oxygen and thereby explain the
484 decreased oxygen utilization rates at this loading rate.

485 The ability of a biofilm to cope with step changes in fluoroacetate loading rates was
486 demonstrated under batch culture conditions (Fig 7). The performance of the biofilm was
487 severely affected during the unbuffered 50 mM fluoroacetate experiment. This was
488 demonstrated to be a pH effect and not a consequence of substrate inhibition. In the 10, 20
489 and 50 mM experiments the bulk liquid glycolate concentration was higher than the bulk
490 liquid fluoroacetate concentration after 3, 6 and 9 h, respectively. However, the concentration
491 of fluoroacetate in the bulk liquid continued to decrease towards zero while the glycolate
492 concentration in the effluent remained constant in the 10 and 20 mM experiments and
493 decreased marginally in the 50 mM experiment. These data show the preferential
494 defluorination of bulk liquid fluoroacetate in the presence of higher concentrations of bulk
495 liquid glycolate, even though the latter can be considered a more readily utilizable energy

source. The presence of a fluoroacetate specific permease might account for this apparent preferential utilization of fluoroacetate, Yu *et al.* [8] have characterised a haloacid permease from *Burkholderia cepacia*. They showed that this permease is a specific transporter for halo-substituted acetate including fluoroacetate but is a relatively poor transporter of glycolate. *P. fluorescens* might possess a similar fluoroacetate specific permease which would help explain the preferential degradation of fluoroacetate over glycolate.

In conclusion this study has shown that a pure culture of *P. fluorescens* was capable of almost complete materialisation of fluoroacetate in the MABR. The accumulation and negative impact of free fluoride within the biofilm has important implications for the biological treatment of organofluorine contaminated wastewater streams. Few studies of xenobiotics treatment in biofilms investigate the fate of intermediate metabolites, an exception being the study by Debus et al. [17]. This omission may potentially be very important as a failure to consider the fate of intermediates in biofilm models may result in the false assumption that some regions of the biofilm are substrate limited.

Acknowledgements

Science Foundation Ireland (SFI) grant 04/BRG/E0072 provided financial support.

References

1. Key, B. D.; Howell, R. D.; Criddle, C. S., Fluorinated organics in the biosphere. *Enviromental Science and Technology* **1997,** 31, (9), 2445-2454.
2. Muller, K.; Faeh, C.; Diederich, F., Fluorine in pharmaceuticals: Looking beyond intuition. *Science* **2007,** 317, (5846), 1881-1886.
3. Isanbor, C.; O'Hagan, D., Fluorine in medicinal chemistry: A review of anti-cancer agents. *Journal of Fluorine Chemistry* **2006,** 127, (3), 303-319.
4. Arellano, M.; Malet-Martino, M.; Martino, R.; Gires, P., The anti-cancer drug 5-fluorouracil is metabolized by the isolated perfused rat liver and in rats into highly toxic fluoroacetate. *British Journal of Cancer* **1998,** 77, (1), 79-86.
5. Tecle, B.; Casida, J. E., Enzymatic defluorination and metabolism of fluoroacetate, fluoroacetamide, fluoroethanol, and (-)-erythro-fluorocitrate in rats and mice examined by F-19 and C-13 NMR. *Chemical Research in Toxicology* **1989,** 2, (6), 429-435.
6. Tisdale, M. J.; Brennan, R. A., Role of fluroacetate in the toxicity of 2-fluroethylnitrosoureas. *Biochemical Pharmacology* **1985,** 34, (18), 3323-3327.
7. Rompp, A.; Klemm, O.; Fricke, W.; Frank, H., Haloacetates in fog and rain. *Environmental Science Technology*, **2001,** *35*, (7), 1294-1298.
8. Yu, M.; Faan, Y.-W.; Chung, W. Y. K.; Tsang, J. S. H., Isolation and characterization of a novel haloacid permease from *Burkholderia cepacia* MBA4. *Applied and Environmental Microbiology.* **2007,** 73, (15), 4874-4880.
9. Natarajan, R.; Azerad, R.; Badet, B.; Copin, E., Microbial cleavage of CF bond. *Journal of Fluorine Chemistry* **2005,** 126, (4), 424-435.
10. Liu, J.-Q.; Kurihara, T.; Ichiyama, S.; Miyagi, M.; Tsunasawa, S.; Kawasaki, H.; Soda, K.; Esaki, N., Reaction mechanism of fluoroacetate dehalogenase from *Moraxella sp*. B. *Journal of Biological Chemistry.* **1998,** 273, (47), 30897-30902.
11. Syron, E.; Casey, E., Membrane-aerated biofilms for high rate biotreatment: Performance appraisal, engineering principles, scale-up, and development requirements. *Environmental Science & Technology* **2008,** 42, (6), 1833-1844.
12. Buer, T.; Adams, N.; Hong, Y., High efficiency oxygen transfer membrane supported biofilm reactor for wastewater treatment. *IWA North American Regional Membrane Research Conference August 10-13,* **2008,** *University of Massachusetts, Amherst.*
13. Hibiya, K.; Terada, A.; Tsuneda, S.; Hirata, A., Simultaneous nitrification and denitrification by controlling vertical and horizontal microenvironment in a membrane-aerated biofilm reactor. *Journal of Biotechnology* **2003,** 100, (1), 23-32.
14. Li, T. G.; Liu, J. X.; Bai, R. B.; Wong, F. S., Membrane-aerated Biofilm reactor for the treatment of acetonitrile wastewater. *Environmental Science & Technology* **2008,** 42, (6), 2099-2104.
15. Terada, A.; Yamamoto, T.; Tsuneda, S.; Hirata, A., Sequencing batch membrane biofilm reactor for simultaneous nitrogen and phosphorus removal: Novel application of membrane-aerated biofilm. *Biotechnology and Bioengineering* **2006,** 94, (4), 730-739.
16. Semmens, M. J.; Dahm, K.; Shanahan, J.; Christianson, A., COD and nitrogen removal by biofilms growing on gas permeable membranes. *Water Research* **2003,** 37, (18), 4343-4350.
17. Debus, O.; Baumgartl, H.; Sekoulov, I., Influence of Fluid Velocities on the Degradation of Volatile Aromatic-Compounds in Membrane-Bound Biofilms. *Water Science and Technology* **1994,** 29, (10-11), 253-262.

18. Delille, A.; Quiles, F.; Humbert, F., In situ monitoring of the nascent P*seudomonas fluorescens* biofilm response to variations in the dissolved organic carbon level in low-nutrient water by attenuated total reflectance-fourier transform infrared spectroscopy. *Applied and Environmental Microbiology* **2007,** 73, 5782-5788.
19. Ternstrom, A.; Lindberg, A. M.; Molin, G., Classification of the spoilage flora of raw and pasteurized bovine-milk, with special reference to Pseudomonas and Bacillus. *Journal of Applied Bacteriology* **1993,** 75, (1), 25-34.
20. Wong, D. H.; Kirkpatrick, W. E.; King, D. R.; Kinnear, J. E., Defluorination of sodium monofluoroacetate (1080) by microorganisms isolated from western Australian soils. *Soil Biology and Biochemistry* **1992,** 24, (9), 833-838.
21. Syron, E.; Casey, E., Model-based comparative performance analysis of membrane aerated biofilm reactor configurations. *Biotechnology and Bioengineering* **2008,** 99, (6), 1361-1373.
22. Casey, E.; Glennon, B.; Hamer, G., Oxygen mass transfer characteristics in a membrane-aerated biofilm reactor. *Biotechnology and Bioengineering* **1999,** 62, (2), 183-192.
23. Lewis, K.; S., W., Determination of glycolic, glyoxylic, and oxalic acids *Methods in enzymology* **1957,** 3, 269-276.
24. Casey, E., Tracer measurements reveal experimental evidence of biofilm consolidation. *Biotechnology and Bioengineering* **2007,** 98, 913-918.
25. Pavasant, P.; dosSantos, L. M. F.; Pistikopoulos, E. N.; Livingston, A. G., Prediction of optimal biofilm thickness for membrane-attached biofilms growing in an extractive membrane bioreactor. *Biotechnology and Bioengineering* **1996,** 52, (3), 373-386.
26. Picioreanu, C.; van Loosdrecht, M. C. M.; Heijnen, J. J., Effect of diffusive and convective substrate transport on biofilm structure formation: A two-dimensional modeling study. *Biotechnology and Bioengineering* **2000,** 69, (5), 504-515.
27. Heffernan, B.; Murphy, C. D.; Casey, E., Comparison of planktonic and biofilm cultures of *Pseudomonas fluorescen*s DSM 8341 cells grown on fluoroacetate. *Applied and Environmental Microbiology* **2009,** 75, (9), 2899-2907.
28. Characklis, W. G., Microbial fouling. In: Characklis,. *W.G., Marshall, K.C. (Eds.), Biofilms. Wiley, New York,* **1990**, (pp. 523-584.).
29. Stoodley, P.; Dodds, I.; Boyle, J. D.; Lappin-Scott, H. M., Influence of hydrodynamics and nutrients on biofilm structure. *Journal of Applied Microbiology* **1999,** 85, 19S-28S.
30. Song, B.; Leff, L. G., Influence of magnesium ions on biofilm formation by *Pseudomonas fluorescens. Microbiological Research* **2006,** 161, (4), 355-361.
31. Donnelly C; Murphy, C. D., Purification and properties of fluoroacetate dehalogenase from *Pseudomonas fluorescens* DSM 8341. *Biotechnol Lett* **2009,** 31, (2), 245-250.
32. Tatevossian, A., Distribution and kinetics of fluoride ions in the free aqueous and residual phases of human dental plaque. *Archives of Oral Biology* **1978,** 23, (10), 893-898.
33. Watson, P. S.; Pontefract, H. A.; Devine, D. A.; Shore, R. C.; Nattress, B. R.; Kirkham, J.; Robinson, C., Penetration of fluoride into natural plaque biofilms. *Journal of Dental Research* **2005,** 84, (5), 451-455.
34. Ahmad, Z.; Senior, A. E., Inhibition of the ATPase activity of *Escherichia coli* ATP synthase by magnesium fluoride. *FEBS Letters* **2006,** 580, (2), 517-520.

612

613

614 **Tables**

615 **Table 1:** Biofilm performance at three different intra-membrane oxygen pressures for reactor
616 II. The fluoroacetate loading rate was maintained at 0.64 mM/h for all intra-membrane
617 pressures. The reactor was operated at steady state for 72 h at each intra-membrane pressure
618 and sampled three times during this time fame.

Pressure (bar)	Oxygen utilization rate ($g/m^2/day$)	Fluoroacetate utilization rate (mM/h)	Glycolate utilization rate (mM/h)	Fluoroacetate concentration (mM)	Glycolate concentration (mM)	Fluoroacetate removal efficiency (%)
0.25	8.8 ± 0.3	0.40 ± 0.06	0.16 ± 0.07	6.3 ± 0.8	7.4 ± 1.7	68.5
0.50	9.2 ± 0.5	0.37 ± 0.05	0.17 ± 0.01	7.1 ± 0.7	6.7 ± 0.9	64.5
0.75	11 ± 0.7	0.40 ± 0.02	0.20 ± 0.05	6.1 ± 0.2	6.2 ± 1.0	69.5

619

620 **Table 2:** Biofilm performance at three different fluoroacetate loading rates, experiments were
621 performed in reactor II. The intra-membrane pressure was 0.50 bar for all fluoroacetate
622 loading rates and the biofilm thickness was 3000 µm. The reactor was operated at steady state
623 for 72 h at each intra-membrane pressure and sampled three times during this time frame.

Loading rate (mM/h)	Oxygen utilization rate ($g/m^2/day$)	Fluoroacetate utilization rate (mM/h)	Glycolate utilization rate (mM/h)	Fluoroacetate concentration (mM)	Glycolate concentration (mM)	Fluoroacetate removal efficiency (%)
0.64	11 ± 2.4	0.33 ± 0.02	0.21 ± 0.08	7.8 ± 0.6	3.7 ± 1.6	61.0
0.40	3.6 ± 1.1	0.32 ± 0.10	0.23 ± 0.15	2.1 ± 1.0	4.4 ± 1.6	89.5
0.32	5.0 ± 1.9	0.23 ± 0.01	0.15 ± 0.05	1.7 ± 0.32	2.6 ± 1.4	91.5

624

Figure legends

Figure 1: Schematic of the membrane-aerated bioreactor (MABR).

Figure 2: Linearised biofilm thickness measurements reveal four distinct phases of biofilm accumulation for reactor I (●) and reactor II (□). For ease of comparison time zero on the *x*-axis is shifted 24 h prior to initial visual observations of biofilm formation. The intra membrane oxygen pressure was 0.25 bar gauge for both experiments.

Figure 3: The effect of biofilm thickness on the oxygen utilization rate during early biofilm growth for reactor I and reactor II. Time zero on the *x*-axis is 24 h prior to initial biofilm formation. The different phases of growth A, B and C are indicated. The intra membrane oxygen pressure was 0.25 bar gauge for both experiments.

Figure 4: Measured (A) and predicted (B) dissolved oxygen profiles at 0.25 (——), 0.5 (••••) and 0.75 (— —) bar within a 3700 μm thick biofilm. The biofilm membrane interface is located at 0 μm on the *x*-axis and the biofilm bulk liquid interface is located at 3700 μm on the *x*-axis.

Figure 5: Measured free fluoride ion (□), fluoroacetate (▲) and glycolate (●) concentrations in the effluent of reactor II and reactor I during early stage of biofilm growth. Time zero on the *x*-axis is 24 h prior to initial biofilm formation.

Figure 6: Predicted profiles of fluoroacetate (——), glycolate (••••), oxygen (— —) free fluoride ion (—••—) and activity (–•–) at three experimental fluoroacetate loading rates (A) 0.64, (B) 0.40 and (C) 0.32 mM/h. The intra-membrane pressure was 0.50 bar for all fluoroacetate loading rates and the biofilm thickness was 3000 μm.

Figure 7: Free fluoride ion (□), fluoroacetate (◇), glycolate (●) and oxygen transfer rates (▲) in batch biofilm experiments performed in reactor II with initial fluoroacetate concentrations of (A) 10, (B) 20, (C) 50 unbuffered and (D) 50 mM buffered. The reactor was operated at steady state conditions for at least 48 h prior to a batch experiment. Time zero on the *x*-axis is

650 the time at which influent feed was discontinued. Biofilm thickness was 3700 μm and the
651 intra-membrane pressure was 0.50 bar.

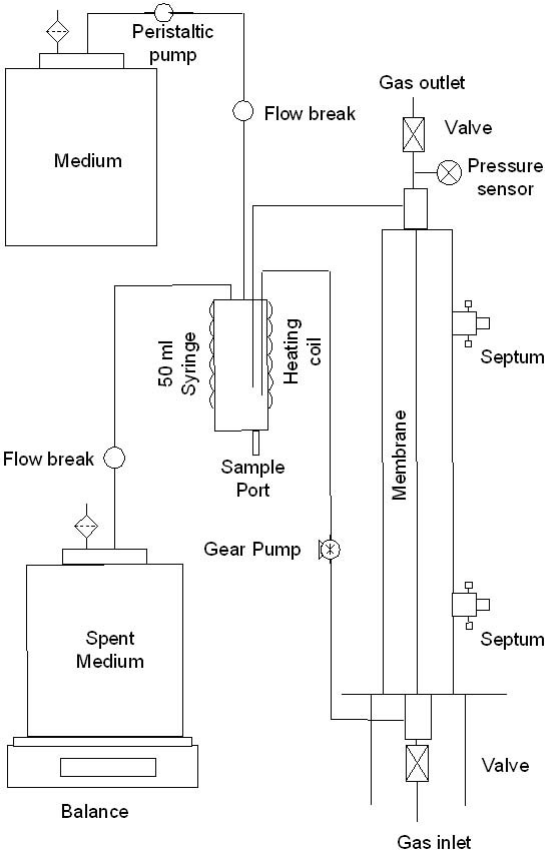
Peristaltic pump
Medium
Flow break
Gas outlet
Valve
Pressure sensor
50 ml Syringe
Heating coil
Septum
Membrane
Flow break
Sample Port
Gear Pump
Spent Medium
Septum
Valve
Balance
Gas inlet

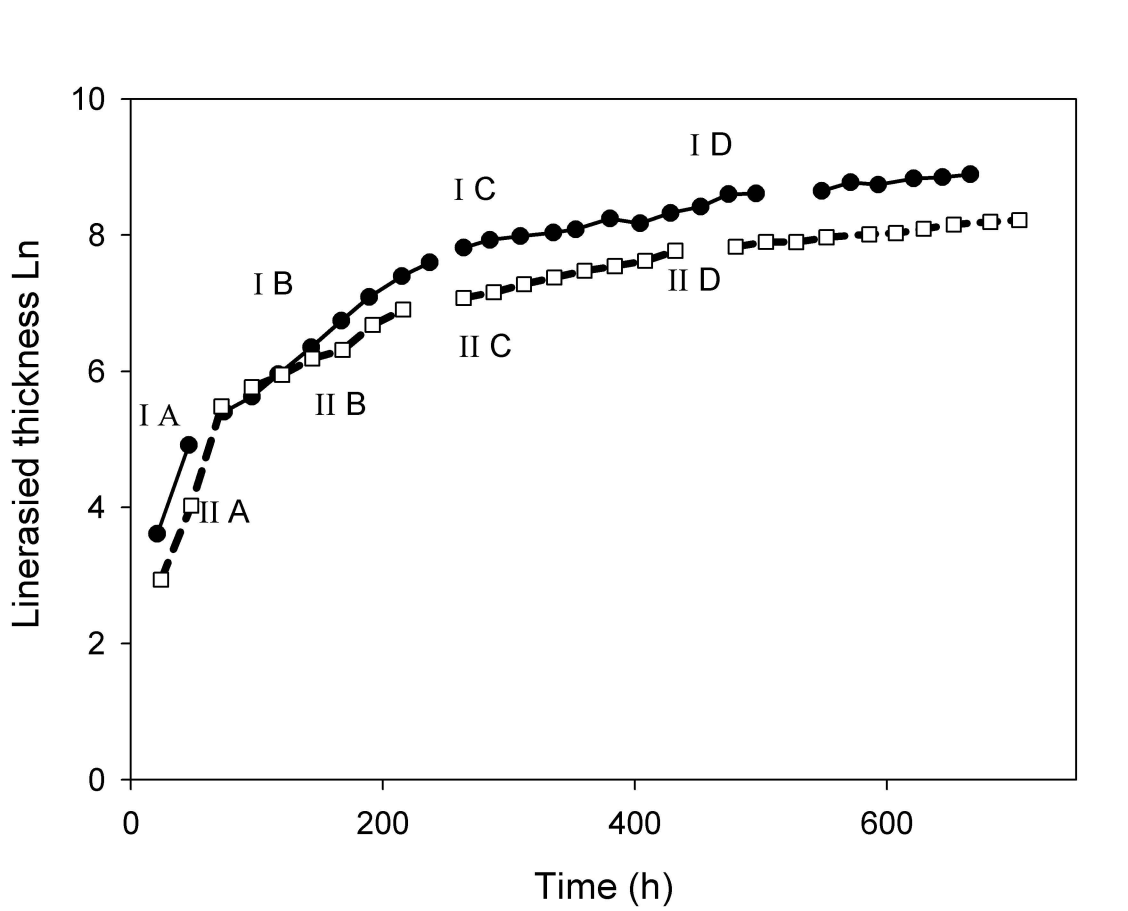
10
8
6
4
2
0
0
200
400
600
Linerasied thickness Ln
Time (h)
I A
II A
I B
II B
I C
II C
I D
II D

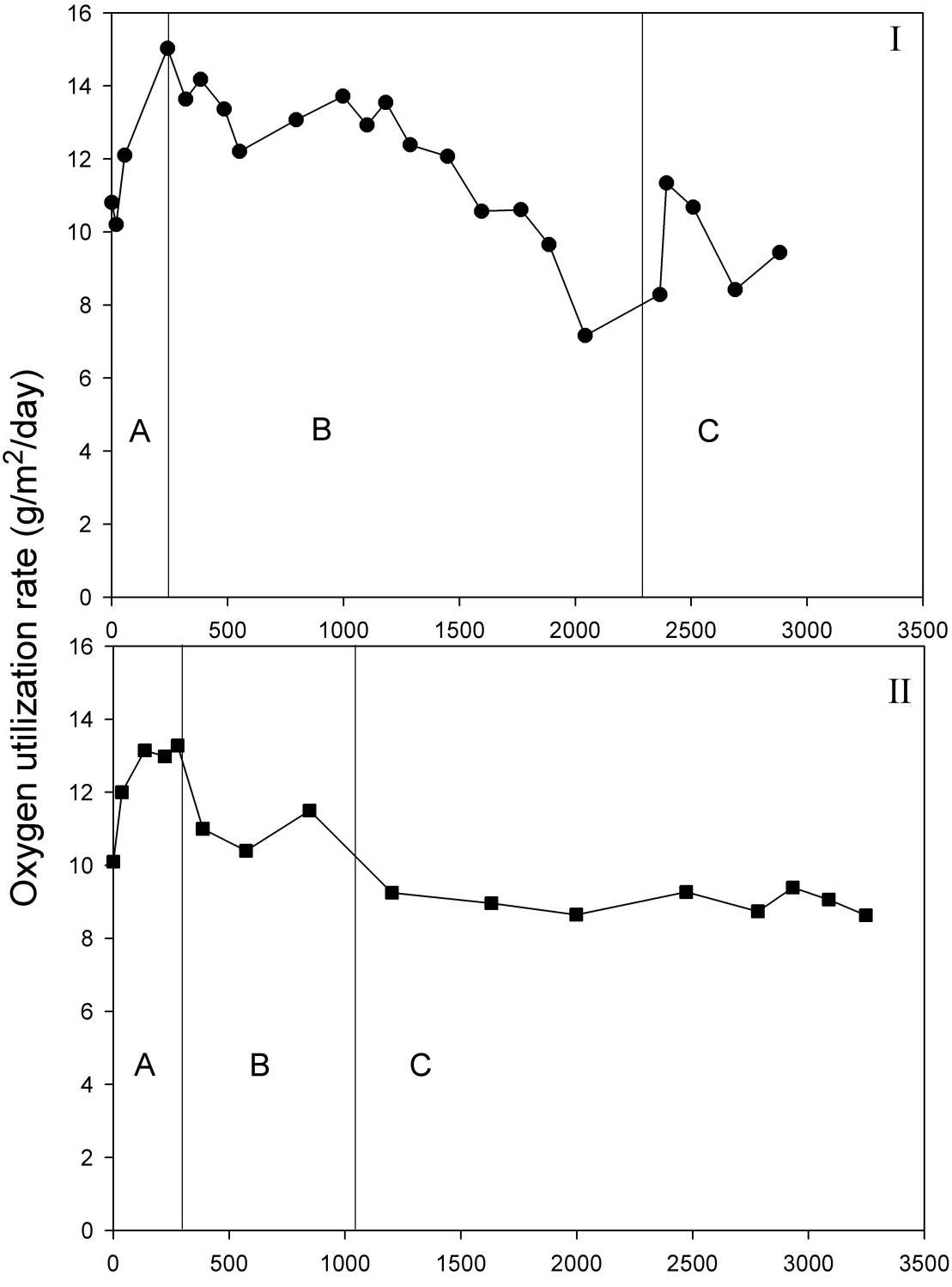
I
II
A
B
C
Oxygen utilization rate (g/m2/day)
Linearised thickness (μm)
0
2
4
6
8
10
12
14
16
500
1000
1500
2000
2500
3000
3500

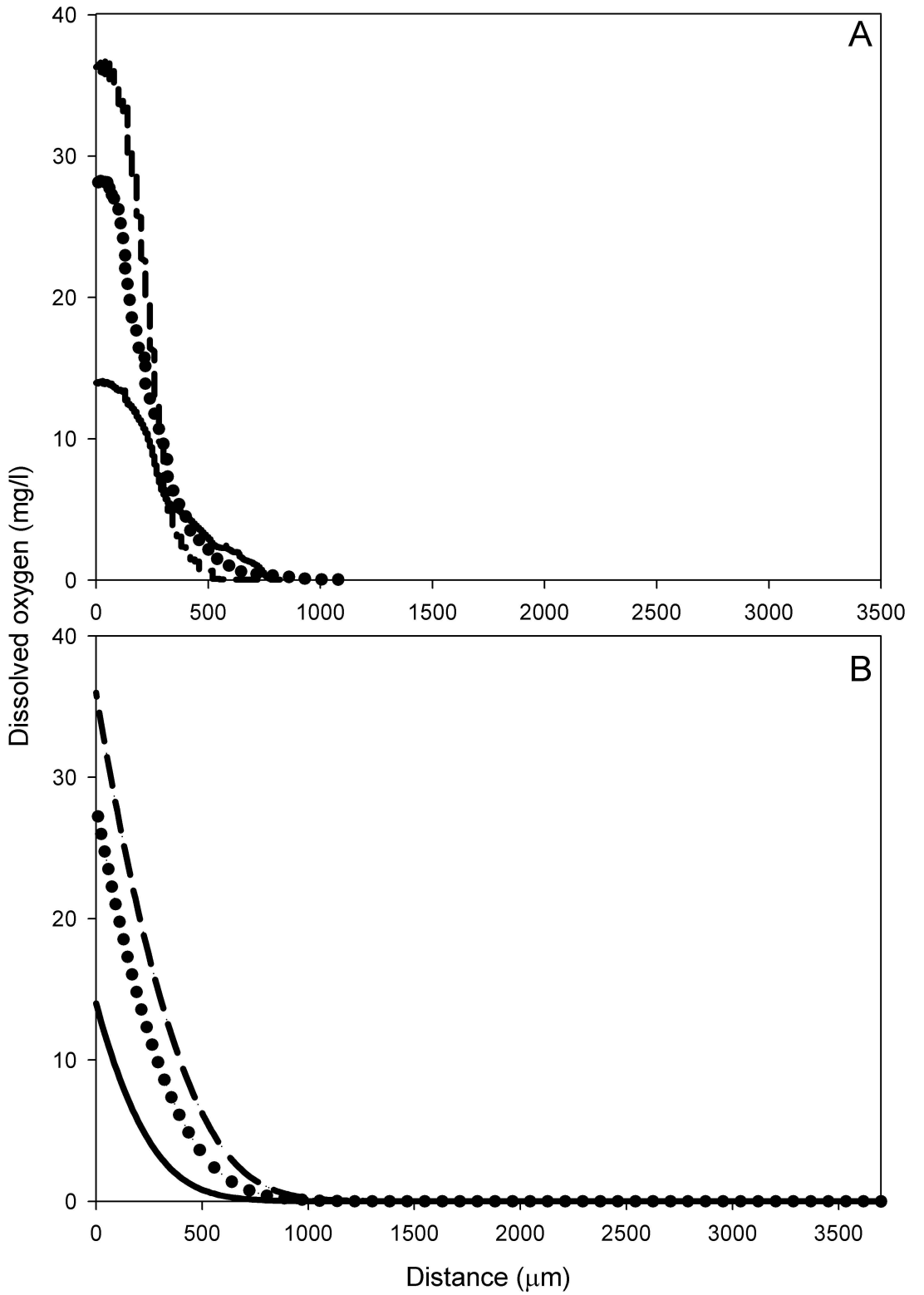
A
B
Dissolved oxygen (mg/l)
Distance (μm)
0
10
20
30
40
0
500
1000
1500
2000
2500
3000
3500

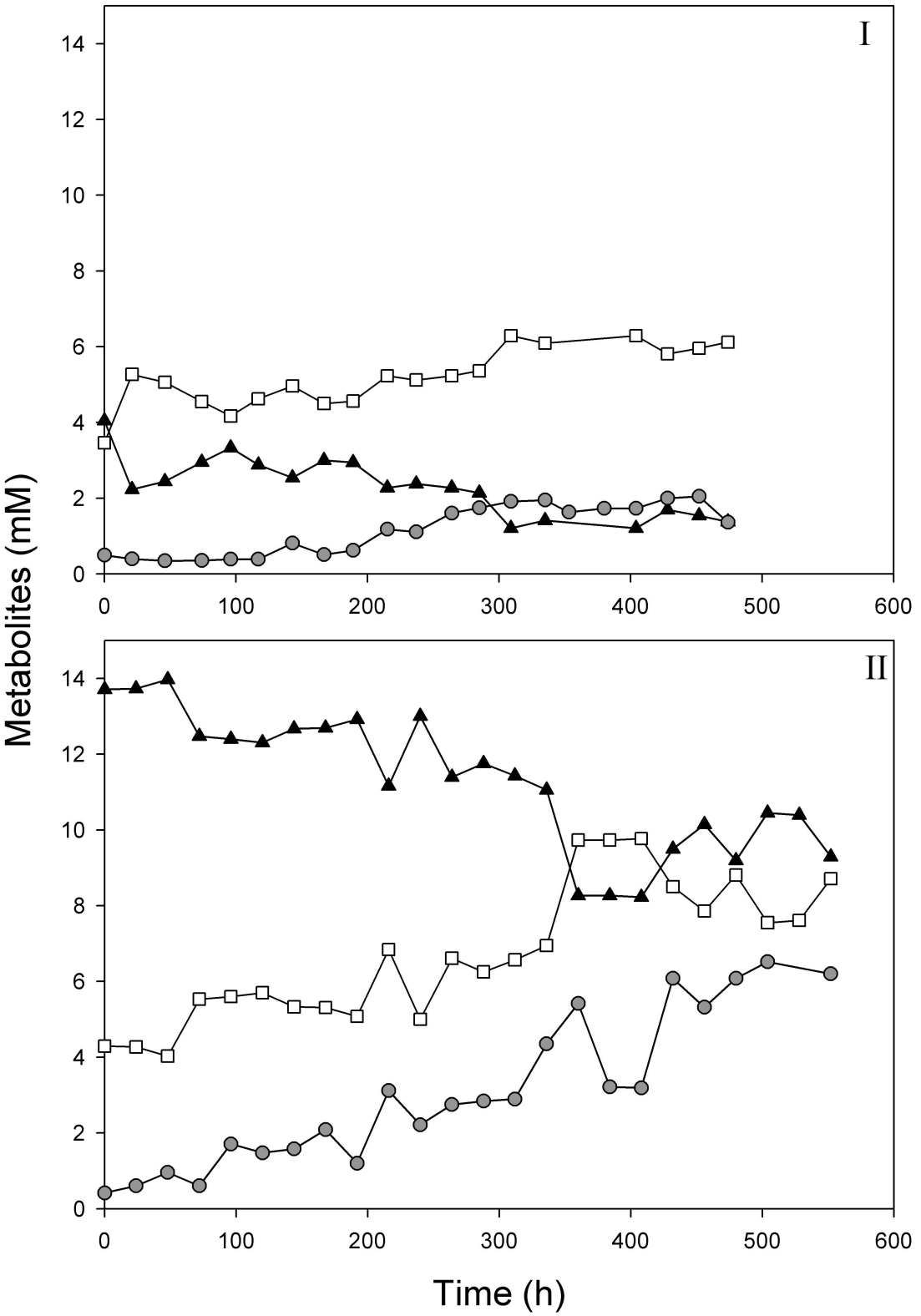
I
II
Metabolites (mM)
Time (h)
0
2
4
6
8
10
12
14
0
100
200
300
400
500
600

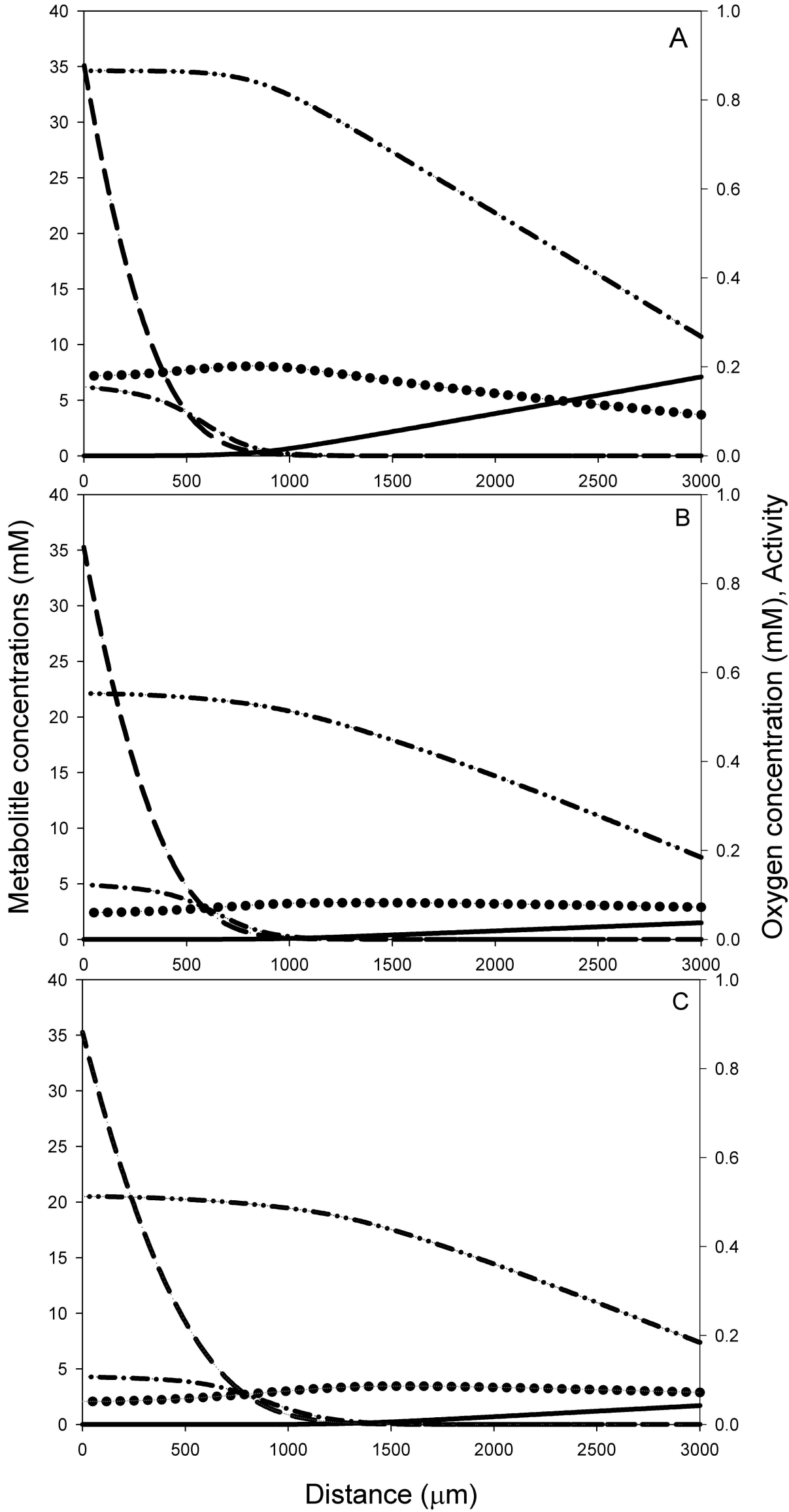
A
B
C
Metabolitle concentrations (mM)
Oxygen concentration (mM), Activity
Distance (μm)
0
5
10
15
20
25
30
35
40
0.0
0.2
0.4
0.6
0.8
1.0
0
500
1000
1500
2000
2500
3000

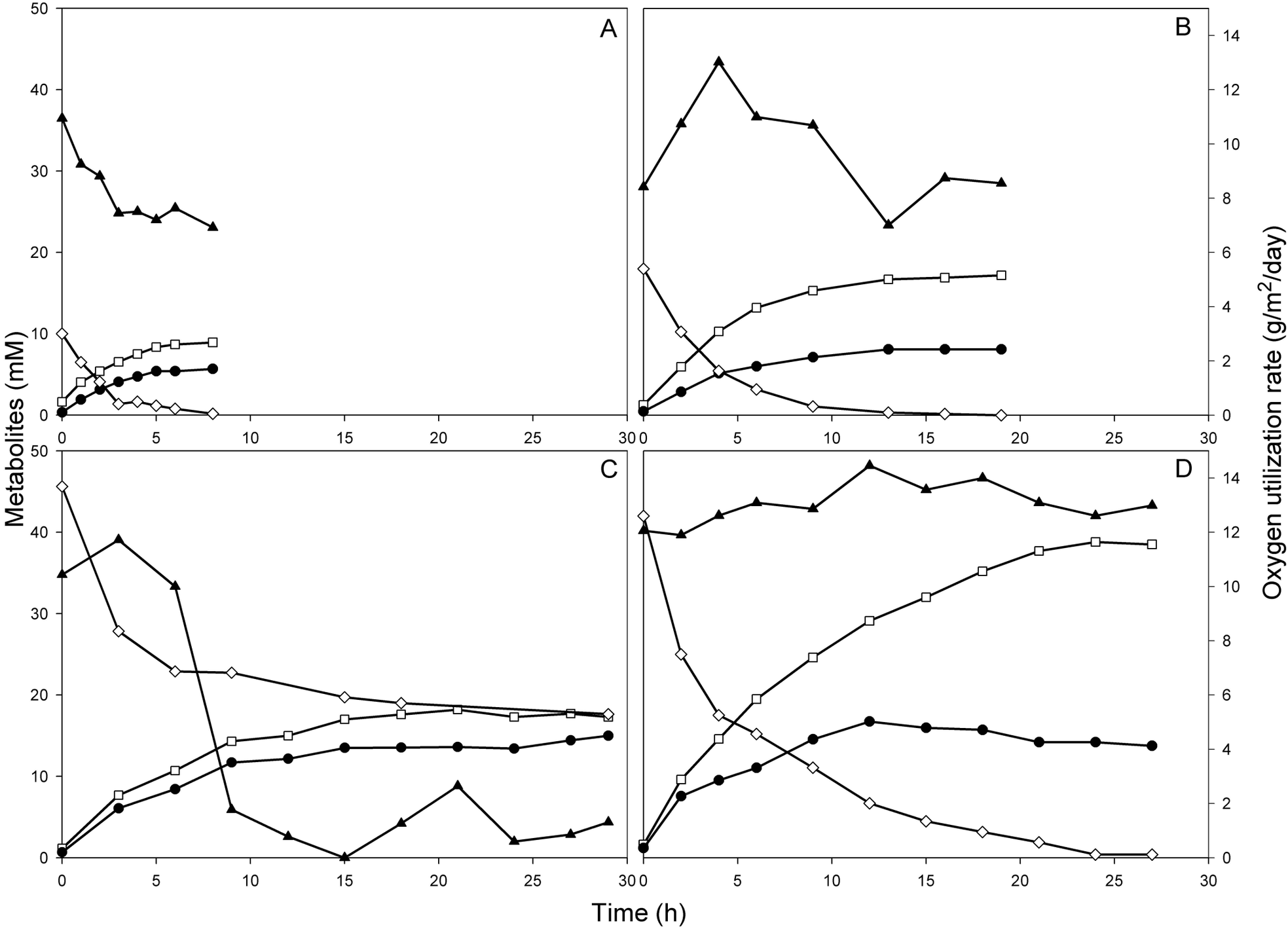
A
B
C
D
Metabolites (mM)
Oxygen utilization rate (g/m2/day)
Time (h)
0
5
10
15
20
25
30
0
10
20
30
40
50
0
2
4
6
8
10
12
14